A&A 585, A125 (2016)
DOI: 10.1051/0004-6361/201525824

Astronomy & Astrophysics

Investigating the cores of fossil systems with *Chandra*

V. Bharadwaj[1], T. H. Reiprich[1], J. S. Sanders[2], and G. Schellenberger[1]

[1] Argelander-Institut für Astronomie, Auf dem Hügel 71, 53121 Bonn, Germany
e-mail: bharadwaj@astro.uni-bonn.de
[2] Max-Planck-Institut für Extraterrestriche Physik, Giessenbachstrasse 1, 85748 Garching, Germany

Received 5 February 2015 / Accepted 9 September 2015

ABSTRACT

Aims. We aim to systematically investigate the cores of a sample of fossil galaxy groups and clusters ("fossil systems"), using *Chandra* data, to see what hints they can offer about the properties of the intracluster medium in these particular objects.
Methods. We chose a sample of 17 fossil systems from literature with archival *Chandra* data and determined the cool-core fraction for fossils via three observable diagnostics, namely the central cooling time, cuspiness, and concentration parameter. We quantified the dynamical state of the fossils by the X-ray peak/brightest cluster galaxy (BCG) separation, and the X-ray peak/emission weighted centre separation. We also investigated the X-ray emission coincident with the brightest cluster galaxy (BCG) to detect the presence of potential thermal coronae. A deprojection analysis was performed for fossils with $z < 0.05$ to resolve subtle temperature structures, and to obtain the cooling time and entropy profiles. We also investigated the $L_X - T$ relation for fossils from the 400d catalogue to test whether the scaling relation deviates from what is typically observed for other groups.
Results. Most fossils are identified as cool-core objects via at least two cool-core diagnostics with the population of weak cool-core fossils being the highest. All fossils have their dominant elliptical galaxy within 50 kpc of the X-ray peak, and most also have the emission weighted centre within that distance. We do not see clear indications of an X-ray corona associated with the BCG unlike coronae observed for some other clusters. Fossils lack universal temperature profiles, with some low-temperature objects generally not showing features that are expected for ostensibly relaxed objects with a cool-core. The entropy profiles of the $z < 0.05$ fossil systems can be described well by a power law with shallower indices than what is expected for pure gravitational processes. Finally, the fossils $L_X - T$ relation shows indications of an elevated normalisation with respect to other groups, which seems to persist even after factoring in selection effects.
Conclusions. We interpret these results within the context of the formation and evolution of fossils, and speculate that non-gravitational heating, and AGN feedback in particular, could have had an impact on the ICM properties of these systems.

Key words. galaxies: groups: general – X-rays: galaxies: clusters – galaxies: clusters: intracluster medium

1. Introduction

Clusters of galaxies are the largest gravitationally bound structures in the Universe, with an aggregate mass between a few times 10^{13} $M_\odot$ and 10^{15} $M_\odot$. Consisting of galaxies, hot X-ray emitting gas (the intracluster medium-ICM), and dominated by dark matter, these objects are unique in their application to study both cosmology and astrophysics. On the lower mass end, these systems are sometimes called groups to indicate a smaller aggregation of galaxies. The distinction between groups and clusters is quite loose, with definitions in literature based on optical richness or simply a mass/temperature cut (e.g. Stott et al. 2012).

An ostensibly special class of systems called as fossil systems exist within the existing division of groups and clusters. Fossil systems are objects dominated by a single, bright, elliptical galaxy and are deficient in other bright galaxies. The first fossil group was reported by Ponman et al. (1994), who showed the existence of a system at redshift 0.171 that had a large, X-ray halo associated with an elliptical galaxy. The fossil nomenclature is used to indicate a class of systems that is a remnant of galaxy merging, with hot X-ray gas and an elliptical galaxy the only remnants of this process. A formal definition for a fossil system was provided by Jones et al. (2003), who defined it as a spatially extended X-ray source with luminosity larger than 10^{42} h_{50}^{-2} erg/s with an optical counterpart wherein the magnitude difference between the first and second brightest galaxy is greater than or equal to 2 in the Johnson R band. Simulations by Dariush et al. (2007) show that systems selected by this criterion represent a class of objects, which assemble a higher fraction of their mass at high redshift as compared to non-fossils, further justifying their tag of being early-forming, old systems. This formal definition, however, is open to contention as pointed out again by Dariush et al. (2010) who argue via simulations that a magnitude difference of 2.5 between the first and fourth brightest galaxy identifies 50% more early formed systems.

The most widely acknowledged formation scenario for these systems is one wherein dynamical friction causes galaxies close to the centre of the group to merge and leaves behind a large elliptical galaxy and a hot X-ray halo (e.g. D'Onghia et al. 2005). An outstanding question is if the properties of fossil systems make them a special class of systems. Also, it is still unclear whether they are the final stages of mass assembly or are merely a temporary state in the formation of larger clusters. La Barbera et al. (2009) argue that fossils are not special, and merely represent the final stages of mass assembly in a region without enough surrounding matter. Simulations by von Benda-Beckmann et al. (2008) claim however, that the fossil phase is temporary and the

Table 1. Sample of fossil systems.

Name	redshift	Literature
NGC 6482	0.0131	Khosroshahi et al. (2004)
NGC 1132	0.0232	Mulchaey & Zabludoff (1999)/Yoshioka et al. (2004)
RX J0454.8-1806	0.0314	Yoshioka et al. (2004)
ESO 306-G 017	0.0358	Sun et al. (2004)
UGC 842	0.045	Voevodkin et al. (2008)/Lopes de Oliveira et al. (2010)
RX J1331.5+1108	0.081	Jones et al. (2003)
cl1159p5531	0.081	Vikhlinin et al. (1999)/Voevodkin et al. (2010)
cl2220m5228	0.102	Voevodkin et al. (2010)
cl1038p4146*	0.125	Voevodkin et al. (2010)
cl1416p2315	0.138	Jones et al. (2003)/Voevodkin et al. (2010)
cl0245p0936	0.147	Voevodkin et al. (2010)
cl1340p4017	0.171	Ponman et al. (1994)/Voevodkin et al. (2010)
RX J2247.4+0337	0.199	Vikhlinin et al. (1999)/Voevodkin et al. (2010)
RX J0825.9+0415	0.225	Eigenthaler & Zeilinger (2009)
RX J1256.0+2556	0.232	Jones et al. (2003)
RX J0801+3603	0.287	Eigenthaler & Zeilinger (2009)
RX J1115.9+0130	0.352	Eigenthaler & Zeilinger (2009)
RX J0159.8-0850	0.405	Eigenthaler & Zeilinger (2009)

Notes. The starred entry represents the system only considered in the $L_X - T$ study. Columns are (1) name of the fossil system; (2) redshift; and (3) literature sources.

magnitude gap would end by renewed infall from the surroundings. Adding to the confusion are results by Proctor et al. (2011), who argue that the high mass-to-light ratios of these systems and their low richness are not predicted by any current model of fossil formation. Pierini et al. (2011) argue that compact groups are the progenitors of low-mass fossils, while more massive fossil systems are formed by an early infall of massive satellites, hinting that a singular explanation for the formation of fossils might be inadequate.

Very few fossil systems have been thoroughly studied, which adds to the lack of sound conclusions on their formation and evolution (e.g. Mulchaey & Zabludoff 1999; Khosroshahi et al. 2004; Sun et al. 2004). X-ray sample studies of fossil systems, which could provide us additional details, are even rarer (e.g. Khosroshahi et al. 2007; Miller et al. 2012; Harrison et al. 2012) and have focused more on global properties, such as X-ray luminosity, temperature, and mass. To date, there has never been a detailed and focused investigation of the cores of a sample of fossil systems in X-rays, particularly with respect to their cool-core properties.

The cores of galaxy clusters and groups offer important hints about the dynamical state of the ICM in the central regions, e.g. systems that are morphologically disturbed, generally have long central cooling times (CCTs) and elevated central entropies as compared to relaxed systems that show much shorter CCTs and lower central entropies. The clusters with the strongest cooling, namely the strong cool core (SCC) clusters, show very short CCTs ($\leq$1 Gyr), low entropies ($\leq$30 keV cm^2), and central temperature drops (Hudson et al. 2010). This is not necessarily true for the group regime, where there are examples of systems that do not show any indication of cool gas in the cores despite short CCTs and low entropies (e.g. Bharadwaj et al. 2014). Feedback also plays an important role in cluster/group cores as without it there would be catastrophic cooling with very high mass deposition rates, inconsistent with observations (e.g. Peterson et al. 2001, 2003; Tamura et al. 2001; Kaastra et al. 2001; Sanders et al. 2008). Where do fossil systems fit in this picture? What hints can the cool core properties of these systems offer in terms of their formation and evolution? These are the questions we attempt to address in this paper.

This paper is organised as follows: Sect. 2 deals with the data and analysis. We present our results and discuss them in Sect. 3. A short summary is presented in Sect. 4. Throughout this work, we assume a ΛCDM cosmology with $\Omega_m = 0.30$, $\Omega_\Lambda = 0.70$ and $h = 0.70$ where $H_0 = 100\,h$ km s^{-1} Mpc^{-1}, unless stated otherwise. All errors are quoted at the 68% level. Log is always base 10 here.

2. Data and analysis

2.1. Sample

We selected a sample of 17 fossil systems and candidates spanning a large redshift range (from ~0.01 to ~0.4) with good quality archival *Chandra* data ($t_{exp} \geq 10$ ks) as required for exploring the properties under consideration here. *Chandra* was preferred over *XMM-Newton* because of its superior spatial resolution that makes it easier to probe the central regions, which is the major focus of the work. Though the systems were categorized as fossil systems through different techniques, the basic selection criteria of a lower X-ray luminosity threshold and a magnitude difference between the first and second brightest galaxies, is qualitatively maintained for all of them. We also endeavoured to study the $L_X - T$ relation for those fossil systems selected from the 400d cluster sample (Sect. 3.6) for which we analysed *XMM-Newton* data for one more fossil group, which was not included for the other studies. Table 1 summarises the basic information of the sample with redshifts and literature sources.

2.2. Basic data reduction

Most of the data reduction steps were similar to those followed in Bharadwaj et al. (2015) and Bharadwaj et al. (2014), and we describe these steps here briefly. *Chandra* interactive analysis of observations (CIAO) 4.4[1] with *Chandra* calibration database (CALDB) 4.5.0 was used for the data reduction for all but one object–cl1416p2315. While the manuscript was under review, a very recent (2014), and much deeper observation

[1] http://cxc.harvard.edu/ciao

of cl1416p2315 was made available in the *Chandra* archives, which we analysed with CIAO 4.7 and CALDB 4.6.7, to account for changes in the Advanced CCD imaging spectrometer (ACIS) time-dependent gain and to use the proper blank-sky background files. This is unlikely to have an effect on other objects in our sample with much older observations, and is already accounted for in CALDB 4.5.0, and therefore we decided not to re-analyse them. Other than these changes, all the steps that were carried out were exactly the same.

The `chandra_repro` task reprocessed the data and removed afterglows, created the bad-pixel table, and applied the calibration. The `lc_clean` algorithm was used to filter the soft proton flares, with the light curves visually inspected to check for any residual flaring. Point sources were detected and excluded from further analysis with the `wavdetect` wavelet algorithm. Since our focus is on the bright, central regions, background subtraction for the spectral and surface brightness analysis was done throughout using the blank sky background files. The X-ray emission peak (EP) was determined in an exposure corrected, point source subtracted image using the CIAO tools built into ds9 with a pixel scale of 2.

For extracting spectra, we created annular regions with a minimum source counts threshold of 1000. This ensured that the annuli are sufficiently small and, at the same time does not sacrifice the signal to noise too much. The resultant spectra were fit with an absorbed Astrophysical plasma emission code (APEC) model in the 0.7–7.0 keV energy range, with the $n_{\rm H}$ value taken from the built-in $n_{\rm H}$ ftools, which output the value from the Leiden/Argentine/Bonn (LAB) survey (Kalberla et al. 2005). The abundance was kept thawed for the spectral fit and in cases where we could not get a reasonable constraint on the value, we froze it to 0.30. We used the Anders & Grevesse (1989) abundance table throughout.

The surface brightness profile (SBP) was obtained by centring on the EP in the 0.5–2.0 keV energy band. This SBP was then fit by a single or double beta model (e.g. Cavaliere & Fusco-Femiano 1976) given by

$$\Sigma = \Sigma_0 \left[1 + \left(\frac{x}{x_{\rm c}}\right)^2\right]^{-3\beta+1/2} \tag{1}$$

$$\Sigma = \Sigma_{01} \left[1 + \left(\frac{x}{x_{\rm c_1}}\right)^2\right]^{-3\beta_1+1/2} + \Sigma_{02} \left[1 + \left(\frac{x}{x_{\rm c_2}}\right)^2\right]^{-3\beta_2+1/2} \tag{2}$$

where $x_{\rm c_i}$ is the core radius. This in turn gave us the electron density profile for the single and double beta cases as

$$n = n_0 \left[1 + \left(\frac{r}{r_{\rm c}}\right)^2\right]^{\frac{-3\beta}{2}} \tag{3}$$

$$n = \left(n_{01}^2 \left[1 + \left(\frac{r}{r_{\rm c_1}}\right)^2\right]^{-3\beta_1} + n_{02}^2 \left[1 + \left(\frac{r}{r_{\rm c_2}}\right)^2\right]^{-3\beta_2}\right)^{1/2} \tag{4}$$

where $r_{\rm c}$ is the physical core radius. The central electron density n_0 for the single beta case is given by:

$$n_0 = \left(\frac{10^{14} 4\pi D_{\rm A} D_{\rm L} \zeta N}{\rm EI}\right)^{\frac{1}{2}}. \tag{5}$$

Here, N is the normalisation of the APEC model in the innermost annulus, ζ is the ratio of electrons to protons (∼1.2), $D_{\rm A}$ is the angular diameter distance and $D_{\rm L}$ is the luminosity distance. EI is defined as:

$$\mathrm{EI} = 2\pi \int_{-\infty}^{\infty} \int_{0}^{R} x \left(1 + \frac{x^2 + l^2}{x_{\rm c}^2}\right)^{-3\beta} \mathrm{d}x\mathrm{d}l \tag{6}$$

where R is the radius of the innermost annulus.

Similarly, for the double beta case, n_0 (Appendix A of Hudson et al. 2010) is given by

$$n_0 = \left[\frac{10^{14} 4\pi(\Sigma_{12}\mathrm{LI}_2 + \mathrm{LI}_1) D_{\rm A} D_{\rm L} \zeta N}{\Sigma_{12}\mathrm{LI}_2\mathrm{EI}_1 + \mathrm{LI}_1\mathrm{EI}_2}\right]^{\frac{1}{2}} \tag{7}$$

with the same definitions as before. $\mathrm{LI_i}$ is the line emission measure and is defined as

$$\mathrm{LI_i} = \int_{-\infty}^{\infty} \left(1 + \frac{l^2}{x_{\rm c_i}^2}\right)^{-3\beta_{\rm i}} \mathrm{d}l \tag{8}$$

To estimate the uncertainty in n_0, we conducted Monte Carlo simulations where the surface brightnesses were varied within their errors to generate new SBPs. These new SBPs were then fit again to a single or double beta model, which was then used to determine n_0 (the APEC normalisation is also varied each time within the errors). The process was repeated 500 times to get a distribution for the values of n_0, and the standard deviation of the distribution gives the uncertainty in the measured n_0.

2.3. Cool-core analysis

The most robust parameter to identify the cool-core nature of an object is the CCT (Hudson et al. 2010), a quantity that is dependent on the central temperature and the central density. Considering that most (59%) of our objects have a redshift ≥0.1, the determination of the CCT becomes problematic given that it is difficult to resolve the temperature profile for these objects in the central regions. Moreover, in some cases the data quality is not good enough to determine a temperature profile. Thus, in addition to the CCT, we used two other diagnostics, namely, cuspiness α and concentration parameter $c_{\rm SB}$, both of which have been shown to have a strong correlation with the cooling time (e.g. Santos et al. 2010; Hudson et al. 2010). Indeed, recent studies of high redshift systems have used these two quantities to identify their cool-core (CC) nature (e.g. Semler et al. 2012; Pascut & Ponman 2015). In our study, if a fossil satisfied two out of three CC diagnostics, it was classified as a CC system.

The CCT is given as

$$\mathrm{CCT} = t_{\rm cool}(0) = \frac{3}{2}\zeta \frac{(n_{\rm e0} + n_{\rm i0}) k T_0}{n_{\rm e0}^2 \Lambda(T_0, Z_0)} \tag{9}$$

where $n_{\rm i0}$ and $n_{\rm e0}$ are the central ion and electron densities, respectively, and T_0 is the temperature in the innermost annulus. As with Hudson et al. (2010) and Bharadwaj et al. (2014), we took the value of central density values to be the value at $r = 0.004 r_{500}$. To estimate r_{500}, we first determined the virial temperature ($T_{\rm vir}$) in a single region centred on the EP, which extended to the outermost boundary of the outermost temperature bin. The size of this region effectively corresponds to $0.3{-}0.5 r_{500}$ for most objects, where the temperature gradient is not too significant (see Fig. 2 right, and Appendix A). We then used the following scaling relation by Evrard et al. (1996) to determine r_{500} following Hudson et al. (2010) and Bharadwaj et al. (2014)

$$r_{500} = 2 \times \left(\frac{T_{\rm vir}}{10\ \mathrm{keV}}\right)^{\frac{1}{2}} \mathrm{Mpc}. \tag{10}$$

Table 2. Cool-core diagnostics of the fossils.

Name	EP (RA/Dec)	$T_{\rm vir}$ (keV)	CCT (in Gyr)	α	$c_{\rm SB}$	CC or not?
NGC 6482	17:51:48.85 +23:04:19.34	$0.75^{+0.0078}_{-0.0079}$	$0.124^{+0.015}_{-0.013}$	$1.46^{+0.01}_{-0.01}$	–	YES
NGC 1132	02:52:51.79 −01:16:29.13	$1.23^{+0.015}_{-0.016}$	$1.18^{+0.18}_{-0.14}$	$0.969^{+0.066}_{-0.066}$	–	YES
RX J0454.8-1806	04:54:52.34 −18:06:55.57	$2.36^{+0.07}_{-0.07}$	$2.81^{+1.38}_{-0.78}$	$0.888^{+0.020}_{-0.020}$	–	YES
ESO 306-G 017	05:40:06.75 −40:50:10.80	$2.71^{+0.07}_{-0.05}$	$0.497^{+0.064}_{-0.057}$	$0.790^{+0.022}_{-0.022}$	–	YES
UGC 842	01:18:53.67 −01:00:06.75	$1.91^{+0.07}_{-0.07}$	$1.75^{+0.22}_{-0.18}$	$1.02^{+0.06}_{-0.06}$	–	YES
RX J1331.5+1108	13:31:29.65 +11:07:57.44	$0.74^{+0.02}_{-0.03}$	$1.01^{+0.38}_{-0.23}$	$1.33^{+0.11}_{-0.11}$	$0.110^{+0.006}_{-0.006}$	YES
cl1159p5531	11:59:52.20 +55:32:06.29	$1.70^{+0.06}_{-0.02}$	$0.261^{+0.032}_{-0.028}$	$1.78^{+0.20}_{-0.20}$	$0.285^{+0.005}_{-0.005}$	YES
cl2220m5228*	22:20:08.64 −52:27:50.33	$4.12^{+0.38}_{-0.35}$	$20.9^{+2.74}_{-2.34}$	$0.264^{+0.037}_{-0.037}$	$0.062^{+0.006}_{-0.006}$	NO
cl1416p2315	14:16:27.39 +23:15:22.59	$3.98^{+0.14}_{-0.14}$	$4.73^{+1.54}_{-1.01}$	$0.548^{+0.053}_{-0.053}$	$0.059^{+0.002}_{-0.002}$	YES
cl0245p0936*	02:45:48.83 +09:36:37.30	$2.45^{+0.38}_{-0.31}$	$4.99^{+0.90}_{-0.76}$	$0.790^{+0.028}_{-0.028}$	$0.116^{+0.012}_{-0.012}$	YES
cl1340p4017*	13:40:32.70 +40:17:39.26	$1.42^{+0.12}_{-0.10}$	$3.29^{+0.53}_{-0.44}$	$0.620^{+0.025}_{-0.025}$	$0.179^{+0.011}_{-0.011}$	YES
RX J2247.4 + 0337*	22:47:27.88 +03:37:00.22	$2.43^{+0.44}_{-0.35}$	$15.9^{+3.58}_{-2.84}$	$0.359^{+0.036}_{-0.036}$	$0.060^{+0.006}_{-0.006}$	NO
RX J0825.9+0415	08:25:57.83 +04:14:47.12	$4.48^{+0.34}_{-0.29}$	$5.16^{+0.76}_{-0.55}$	$0.460^{+0.071}_{-0.071}$	$0.086^{+0.006}_{-0.006}$	YES
RX J1256.0 + 2556*	12:56:02.25 +25:56:35.38	$3.13^{+0.75}_{-0.51}$	$24.2^{+5.15}_{-3.84}$	$0.250^{+0.045}_{-0.045}$	$0.074^{+0.010}_{-0.010}$	NO
RX J0801+3603	08:00:56.81 +36:03:23.67	$7.43^{+0.29}_{-0.30}$	$2.25^{+0.32}_{-0.24}$	$0.822^{+0.039}_{-0.039}$	$0.120^{+0.003}_{-0.003}$	YES
RX J1115.9+0130	11:15:51.80 +01:29:55.48	$7.12^{+0.26}_{-0.26}$	$0.629^{+0.039}_{-0.037}$	$1.20^{+0.03}_{-0.03}$	$0.224^{+0.005}_{-0.005}$	YES
RX J0159.8-0850	01:59:49.36 −08:49:59.45	$8.46^{+0.39}_{-0.33}$	$0.598^{+0.040}_{-0.038}$	$1.10^{+0.02}_{-0.02}$	$0.223^{+0.006}_{-0.006}$	YES

Notes. The columns are (1) name of system; (2) coordinates (J2000) of the EP; (3) virial temperature of fossil; (4) central cooling time; (5) cuspiness; (6) concentration parameter, (7) cool-core or not, via any two diagnostics. Starred entries represent fossils for which the CCT was determined using $T_{\rm vir}$.

To determine $T_{\rm vir}$ for Cl1038p4146, we used the *XMM-Newton* data sets, which were analysed with the standard pipelines as illustrated in Schellenberger et al. (2015). Spectrum was once again extracted in a single region centred on the EP. Temperatures determined from *Chandra* and *XMM-Newton* can differ significantly as shown by Schellenberger et al. (2015) and hence to remain consistent, we used the formula given in that study to convert the *XMM-Newton* temperature to *Chandra* temperature

$$\log_{10}(T_{\rm XMM}) = 0.889 \times \log_{10}(T_{\rm Chandra}). \quad (11)$$

There are five fossil systems for which we could not obtain a temperature profile. Hence, for these objects we assumed $T_{\rm vir}$ to be the central temperature while constraining the CCT. To estimate the uncertainties in the CCT for these objects, we conservatively assumed the lower bound of the temperature to be 0.6 times of $T_{\rm vir}$ (the largest central temperature decrement observed for nearby fossils, i.e. ES0306) and the upper bound to be 1.25 times $T_{\rm vir}$ (the largest central temperature increment, i.e. NGC 6482). A CC system has a CCT < 7.7 Gyr.

The cuspiness α (Vikhlinin et al. 2007) is defined as:

$$\alpha = -\frac{{\rm d}\log(n)}{{\rm d}\log(r)} \quad (12)$$

which in model parameters, (Hudson et al. 2010) for the single beta model are expressed as

$$\alpha = \frac{3\beta r^2}{r_{\rm c}^2 + r^2} \quad (13)$$

and, for the double beta model are:

$$\alpha = 3r^2 \frac{\Sigma_{12}{\rm LI}_2\beta_1 r_{\rm c_1}^{-2} b_1' + {\rm LI}_1\beta_2 r_{\rm c_2}^{-2} b_2'}{\Sigma_{12}{\rm LI}_2 b_1 + {\rm LI}_1 b_2}. \quad (14)$$

Here, Σ_{12}, ${\rm LI}_1$ and ${\rm LI}_2$ are as defined for the CCT, $b_{\rm i}$ and $b_{\rm i}'$ are defined as

$$b_{\rm i} \equiv \left(1 + \left(\frac{r}{r_{\rm c_i}}\right)^2\right)^{-3\beta_{\rm i}} \quad (15)$$

and

$$b_{\rm i}' \equiv \left(1 + \left(\frac{r}{r_{\rm c_i}}\right)^2\right)^{-3\beta_{\rm i}-1} \quad (16)$$

respectively. In both single and double beta cases, $r = 0.04r_{500}$. A CC system has $\alpha \geq 0.5$. The error on α is once again determined by Monte Carlo simulations as with n_0.

The concentration parameter $c_{\rm SB}$ (Santos et al. 2008) is given as

$$c_{\rm SB} \equiv \frac{\Sigma(r < 40\ {\rm kpc})}{\Sigma(r < 400\ {\rm kpc})} \quad (17)$$

where Σ is the integrated surface brightness within the defined radii (40 and 400 kpc). A CC system has $c_{\rm SB} \geq 0.075$. As the $z < 0.05$ fossils are too close to estimate the surface brightness within 400 kpc, we did not determine $c_{\rm SB}$ for these systems.

3. Results and discussion

3.1. Cool core properties

Table 2 summarises the CC properties of the fossil systems. We find that 14 out of 17 systems, i.e. 82% are cool core systems, as evidenced by at least two out of the three CC diagnostics. If one uses the CCTs, we observe a range of values from a minimum of 0.124 Gyr to a maximum of 24.2 Gyr. The subclassifications of the fossil systems using just the CCTs are 29%

strong cool-core (SCC, CCT < 1 Gyr), 53% weak cool-core (WCC, 1 ≤ CCT < 7.7 Gyr), and 18% non cool-core (NCC, CCT ≥ 7.7 Gyr).

As we have already pointed out, it is not always possible to determine the CCT, and this becomes especially true for X-ray survey data (e.g. eROSITA). Thus, we also state the effect of using one CC parameter alone. With only the cuspiness, we identify 76% of the fossil systems as CC systems. If one uses the concentration parameter alone, we observe that 67% of the systems are selected as CC systems (though it is quite likely that the $z < 0.05$ fossils also have $c_{SB} > 0.075$, in which case the fraction would go up to 76%).

Thus, if one were to simply use a single quantity to identify CC groups, conservatively, one would get a lower limit on the fossil CC fraction of 67% and an upper limit of 82%, i.e. qualitatively there are indications that a majority of fossil systems are CC systems, albeit as the cooling times indicate, most seem to be WCC systems. Figure 1 shows the relation between the CCT–α and CCT–c_{SB} and despite the scatter, it is clear that the anti-correlation trend between the quantities is quite strong with Spearman correlation coefficients of −0.91 and −0.80, respectively.

Assuming no significant effect of selection bias on the sample, to the best of our knowledge, this is the first demonstrated result that suggests that most fossils are in fact cool-core systems based on observable diagnostics. The fraction of cool-core fossil systems is marginally higher than that typically reported for objectively selected group (77%, Bharadwaj et al. 2014) and cluster samples (72%, Hudson et al. 2010), though we do point out that studies have shown that cool-core fractions are generally over-estimated in flux-limited samples of clusters (e.g. Hudson et al. 2010; Eckert et al. 2011; Mittal et al. 2011). The high cool-core fossils fraction is not totally unexpected, as it is generally assumed that fossils are among the most relaxed clusters/groups in the Universe, and hence should have pronounced cool-cores with very short CCTs. What is more intriguing is the fact that the WCC fraction is the highest among the three classes, and the population of WCC and NCC fossils combined together (collectively called non-strong cool-cores; NSCCs) *exceed* the SCC fossils population. This is not what one would naively expect from ostensibly relaxed objects such as these, and these are first indications of the impact of non-gravitational processes on the fossil ICM.

3.2. EP-BCG/EP-EWC separation

We also quantified the dynamical state of the fossil system via two properties, namely the emission peak-emission weighted centre (EWC) separation and the central elliptical galaxy-EP separation, i.e. the BCG-EP separation. These are reasonable indicators of whether the system is relaxed or not, as large values for these numbers would indicate a disturbed system (e.g. Hudson et al. 2010).

The EWC was determined iteratively in a point source subtracted, exposure-corrected image by starting off from the EP following Hudson et al. (2006). The positions of the BCG were taken from literature and was confirmed from the NASA extragalactic database (NED)[2].

Table 3 shows the EP–EWC and EP-BCG separation. All fossils have their BCG located within 50 kpc of the X-ray peak. The EP-EWC peak shows a wider range of values with four fossils (24%) having a separation ≥50 kpc. There is an anti-correlation trend in the EP-EWC separation with the cuspiness with a Spearman correlation coefficient of -0.86, i.e. cool-core fossils have a smaller separation and vice-versa (Fig. 2, left)

Even though the EP-EWC separation of most fossils is less than 50 kpc, again such a large variation in EP-EWC values is not naively expected for ostensibly relaxed systems such as fossils.

Table 3. EP-BCG, EP-EWC separation.

Name	BCG-EP (kpc)	EP-EWC (kpc)
NGC 6482	0.212	1.16
NGC 1132	0.785	5.90
RX J0454.8-1806	3.22	13.3
ESO 306-G 017	0.842	13.3
UGC 842	0.960	2.87
RX J1331.5+1108	1.71	14.8
cl1159p5531	3.77	4.40
cl2220m5228	3.71	62.8
cl1416p2315	0.964	31.6
cl0245p0936	2.78	32.4
cl1340p4017	3.46	30.4
RX J2247.4+0337	2.93	59.2
RX J0825.9+0415	3.58	52.0
RX J1256.0+2556	6.6	61.2
RX J0801+3603	1.29	29.5
RX J1115.9+0130	7.88	21.4
RX J0159.8-0850	4.31	19.5

Notes. The columns are (1) name of system; (2) separation between BCG and EP in kpc; (3) separation between EP and EWC in kpc. The uncertainty in these quantities corresponds to 1″, which in turn corresponds to 0.27 kpc for the nearest fossil, and 5.41 kpc for the furthest fossil.

3.3. Temperature profiles

The right side of Fig. 2, and Appendix A shows the scaled temperature profiles for the fossil systems for which we could obtain one (12 objects). There is a high degree of variation in the profile shapes with temperature drops and flat shapes for the fossil systems and we fail to pinpoint a "typical" temperature profile for the fossils. The high redshift, high-temperature systems show temperature profiles that are expected for a SCC/WCC cluster, i.e. indications of a temperature drop for the SCC objects and a relatively flat profile for the WCC objects (Hudson et al. 2010). NGC 6482 shows a profile that rises all the way to the centre, which has been reported thoroughly in previous studies of the object (Khosroshahi et al. 2004). NGC 1132 shows an almost flat profile with barely a decline towards the centre. ESO306, RX J0454.8-1806, and UGC00842 lack a smooth temperature decline towards the centre, which, while potentially indicative of a cool-core, shows that it is truncated. One possibility for the shape of this temperature profile could be emission from the BCG, which we discuss in Sect. 3.4. A deprojection analysis (Sec. 3.5) for the $z < 0.05$ systems indicates the imprint of a heating process such as AGN. Indeed, only cl1159p5531 shows the "classic", peaky temperature profile observed for low-temperature groups with a SCC (e.g. Sun et al. 2009; Eckmiller et al. 2011) versus that for SCC clusters, which show flattening at intermediate radii. (e.g. Vikhlinin et al. 2006).

[2] http://ned.ipac.caltech.edu/

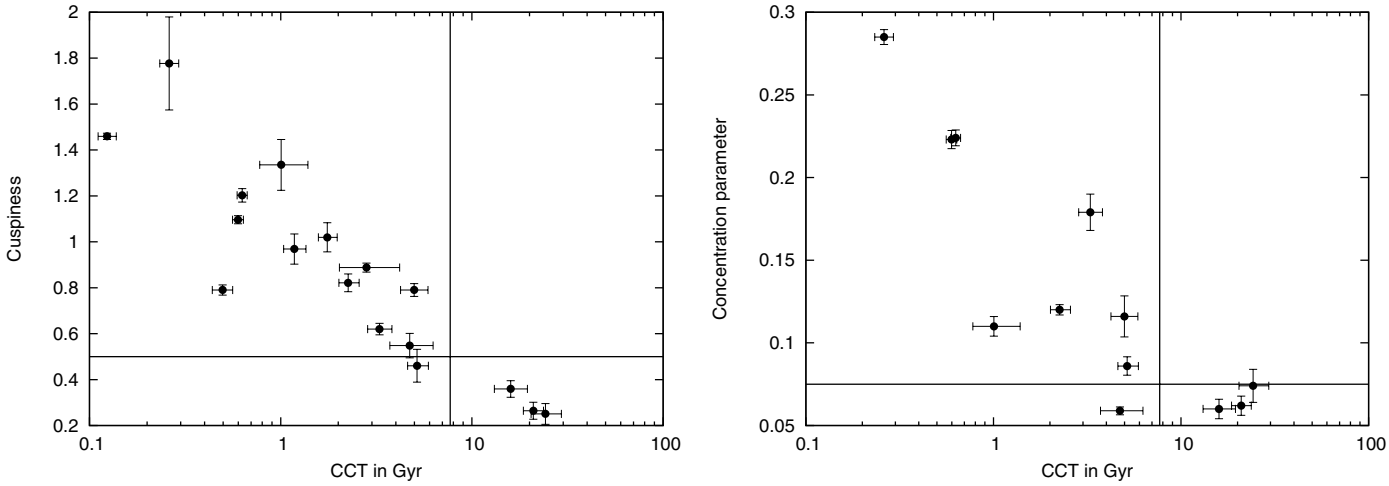

Fig. 1. CCT vs. cuspiness (*left*) and CCT vs. concentration parameter (*right*). The horizontal lines represent the cut for being classified as a cool-core system. The vertical line represents CCT = 7.7 Gyr.

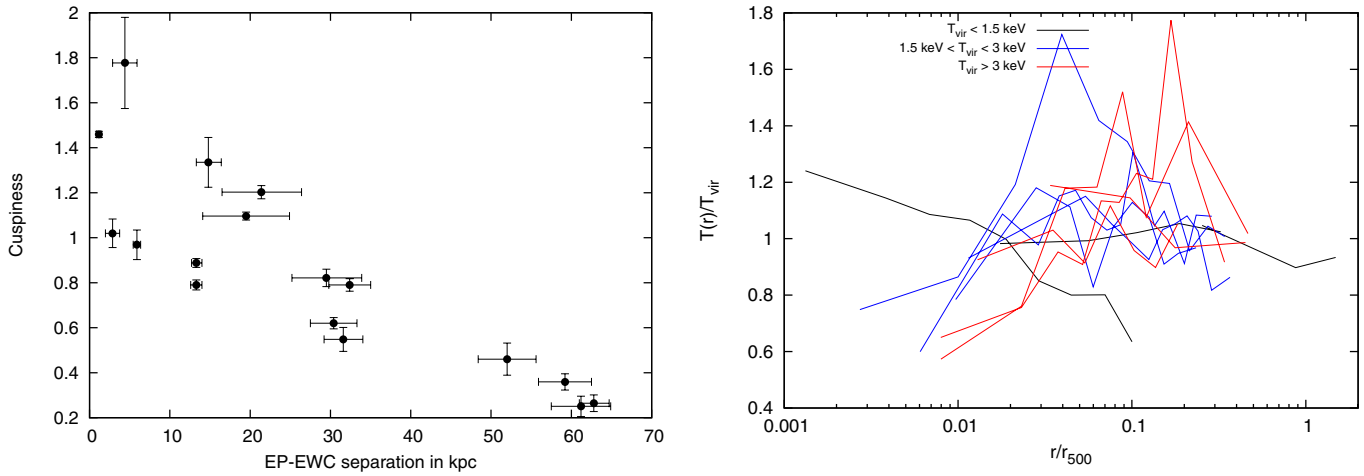

Fig. 2. *Left*: EP-EWC separation and cuspiness. *Right*: scaled temperature profiles colour-coded as a function of virial temperature.

3.4. Potential emission from the BCG

As shown in Table 3, most fossils have a BCG that is very close to or on the X-ray peak. The source detection tool `wavdetect` manages to detect sources that seem to be coincident with the BCG in most cases and we explored whether part of the emission in the core regions comes from the BCG itself, i.e. if they are coronae that consist of gas of stellar origin. This could in principle also explain the truncated "cool-cores" seen in objects, such as UGC00842, ESO306, and RX J0454.8-1806. To study this emission, we focused our attention only on the fossil systems with $z < 0.1$, as it becomes harder to resolve potential coronae for high redshift objects. Using the regions generated by `wavdetect`, we extracted spectra which were then fit by an absorbed APEC model. The regions used for the spectral extraction are of the order of a few kpc, which is the typical size of a corona. We kept the temperature, abundance, and normalisation as the free parameters. The best-fit values were used to determine the X-ray luminosity using *X*spec in the 0.5–2.0 keV band, which was then compared with the ROSAT luminosity of the fossil to determine the strength of this "corona" emission.

Our estimated temperatures from the spectral fit is in most cases much higher (≥1 keV) than is typically observed for the corona class. Moreover, the X-ray luminosity of the emission is in the order of 10^{41} erg/s, which is an order of magnitude higher than typically observed for coronae (Sun et al. 2007) and can account for as much as 17% of the total fossil ROSAT luminosity. Finally, the abundances are much lower (median of 0.28) than has been reported for true coronae (0.8, Sun et al. 2007), which gives indications that the detected emission might not be completely of stellar origin, although we do point out that there is evidence from literature for low-metallicity coronae as well (e.g. Sanders et al. 2014b). One strong possibility is that the stellar content has mixed with the surrounding dense ICM. Table 4 shows the properties of the emission associated with the BCG.

3.5. Deprojection analysis of $z < 0.05$ fossils

To explore thermodynamic properties of fossil systems in detail, we focused in particular on the low redshift ($z < 0.05$) fossils (five in total, namely, NGC 6482, NGC 1132, ESO306, RXJ 0454.8-1806, UGC 00842) and performed a deprojection analysis. To accomplish this, we adopted the MBPROJ code (Sanders et al. 2014a), which is based on the surface brightness deprojection method of Fabian et al. (1981) and is used to

Table 4. X-ray emission coincident with the BCG for $z \leq 0.1$ fossils.

Name	T	$Z_\odot$	$L_X(0.5-2.0\ \mathrm{keV})(10^{41}\ \mathrm{erg/s})$	% of ROSAT group emission
NGC 6482	$0.95^{+0.022}_{-0.022}$	$0.28^{+0.08}_{-0.06}$	1.05	17%
NGC 1132	$0.82^{+0.06}_{-0.08}$	$0.11^{+0.05}_{-0.04}$	1.78	3.8%
RX J0454.8-1806	$1.04^{+0.16}_{-0.08}$	$0.40^{+0.55}_{-0.19}$	1.06	1.2%
ESO 306-G 017	$1.30^{+0.04}_{-0.05}$	$0.29^{+0.12}_{-0.09}$	6.46	2.4%
UGC 842	$1.39^{+0.13}_{-0.07}$	$0.21^{+0.11}_{-0.07}$	1.78	7.1%
RX J1331.5+1108	$0.89^{+0.063}_{-0.034}$	$0.15^{+0.54}_{-0.10}$	1.84	2.9%
cl1159p5531	$1.28^{+0.02}_{-0.02}$	$0.38^{+0.06}_{-0.05}$	17.2	15%

Notes. Columns are (1) name of group; (2) temperature; (3) metallicity; (4) X-ray luminosity from Xspec; (5) "corona" luminosity as percentage of ROSAT luminosity.

estimate the ICM thermodynamical properties from the surface brightness profiles. This method potentially has the advantage of resolving the extreme inner regions of the galaxy group, which cannot be probed with traditional spectral analysis in the absence of very high quality data. Additionally, this is a good opportunity to test the code on low-temperature groups to see how well the results agree with spectral analysis and to test the usability of the code for situations where spectral analysis would not be possible (e.g. survey data).

For purposes of brevity we refrain from describing the code in detail, which is described in the aforementioned paper. The relevant information for this particular study are as follows:

- Surface brightness profiles were extracted in the 0.5−1, 1−1.5, 1.5−2.5, 2.5−7 keV bands.
- We focused only on the "null potential" case for this particular study. This particular case does not assume hydrostatic equilibrium and essentially corresponds to low-resolution spectral fitting. The advantage of this case is that it prevents the thermodynamic profiles from being biased due to assumption of hydrostatic equilibrium. The null potential case can be used to estimate thermodynamic properties with and without linear interpolation of the temperatures between the bins. The non-interpolation case assumes the temperature is the same in groups of three density bins. For the scientific discussion here, we only focused on the profiles that do not involve linear interpolation of the temperatures.
- The abundance is assumed to be 0.3 $Z_\odot$ throughout.

Figure 3 shows a comparison of the temperature profiles from the spectral analysis and MBPROJ. The code does a good job of recovering the shape of the temperature profiles though some deviations are seen for NGC 1132 and NGC 6482, which could be due to the extremely low temperatures of these systems (1.2 and 0.75 keV respectively) and possible projection effects. For the hotter groups, the agreement is much better. Overall though, MBPROJ seems to be a competitive code even on the group regime and would be particularly useful for eROSITA data where most systems would be galaxy groups and would lack sufficient counts for a direct spectral temperature estimate (Borm et al. 2014).

Figure 4 shows the cooling time and entropy profiles of the fossil systems. The cooling time profiles can be well described by a power law with an index varying from 1.06 ± 0.03 to 1.20 ± 0.05 for the five systems. Hudson et al. (2010) define the cooling radius as the radius at which $t_{\mathrm{cool}} = 7.7$ Gyr. For these five fossils, namely, NGC 1132, RX J0454.8-1806, ESO306, NGC 6482, and UGC 00842, this corresponds to 43 kpc, 36 kpc, 51 kpc, 54 kpc, and 30 kpc respectively. However, as shown in Fig. 3, the region with the cool gas (if present) is generally much smaller than the cooling radius. MBPROJ detects cool gas out to 3 kpc for NGC 1132, 12 kpc for RX J0454.8-1806, 9 kpc for ESO306, 0 kpc for NGC 6482, and 19 kpc for UGC 00842. Thus, all these systems seem to lack a group-sized cool-core, and the region of cool gas is not commensurate to the region of short cooling times. As argued above, it seems unlikely that the cool gas component is emission purely associated with the BCG.

The derived entropy profiles can also be well described by a power law of the form $K(r) = K_{100} \times (r/100\ \mathrm{kpc})^m$, as has been used in studies such as e.g. Cavagnolo et al. (2009) and Panagoulia et al. (2014). When the profile is fit with the above function, we obtain a power-law index that is substantially lower than 1.1, which is expected for pure gravitational processes (e.g. Tozzi & Norman 2001). Cavagnolo et al. (2009) also fit their entropy profiles with a power-law model with an additional component for a non-zero core entropy, i.e. $K(r) = K_0 + K_{100} \times (r/100\ \mathrm{kpc})^m$. We also added this component to see if it has an effect on the fitted entropy profile. As shown in Table 5, the index is still much lower than 1.1, and in some cases, K_0 takes unphysical negative values. Qualitatively, this agrees with the results of Panagoulia et al. (2014), who showed that the entropy profiles of a sample of galaxy groups and clusters can be sufficiently described by only a powerlaw without indications of any core-flattening. We also compared the scaled entropy profiles to the baseline entropy profile of Pratt et al. (2010), which is defined as

$$K(R)/K_{500} = 1.42(R/R_{500})^{1.1} \tag{18}$$

where K_{500} is as defined in Pratt et al. (2010) and is dependent on M_{500}. To estimate M_{500}, we used the $M_{500} - T$ scaling relation from Arnaud et al. (2005). As is evident in Fig. 4, there is a significant entropy excess over the baseline entropy profile for the fossils within the radial ranges probed here, and the profile is considerably flatter as compared to the baseline profile. The shallow slopes, and the elevated entropies over a substantially large radial range is indicative of a strong influence of non-gravitational processes on the properties of the ICM, which we discuss in greater detail in Sect. 3.7.

3.6. The $L_X - T$ relation for 400d fossil systems

The $L_X - T$ relation is an interesting scaling relation, which can offer insights into the baryonic physics at play in the ICM, as the physics affects both quantities, T and L_X. For example, clusters with cool-cores/non-cool cores have $L_X - T$ relations with

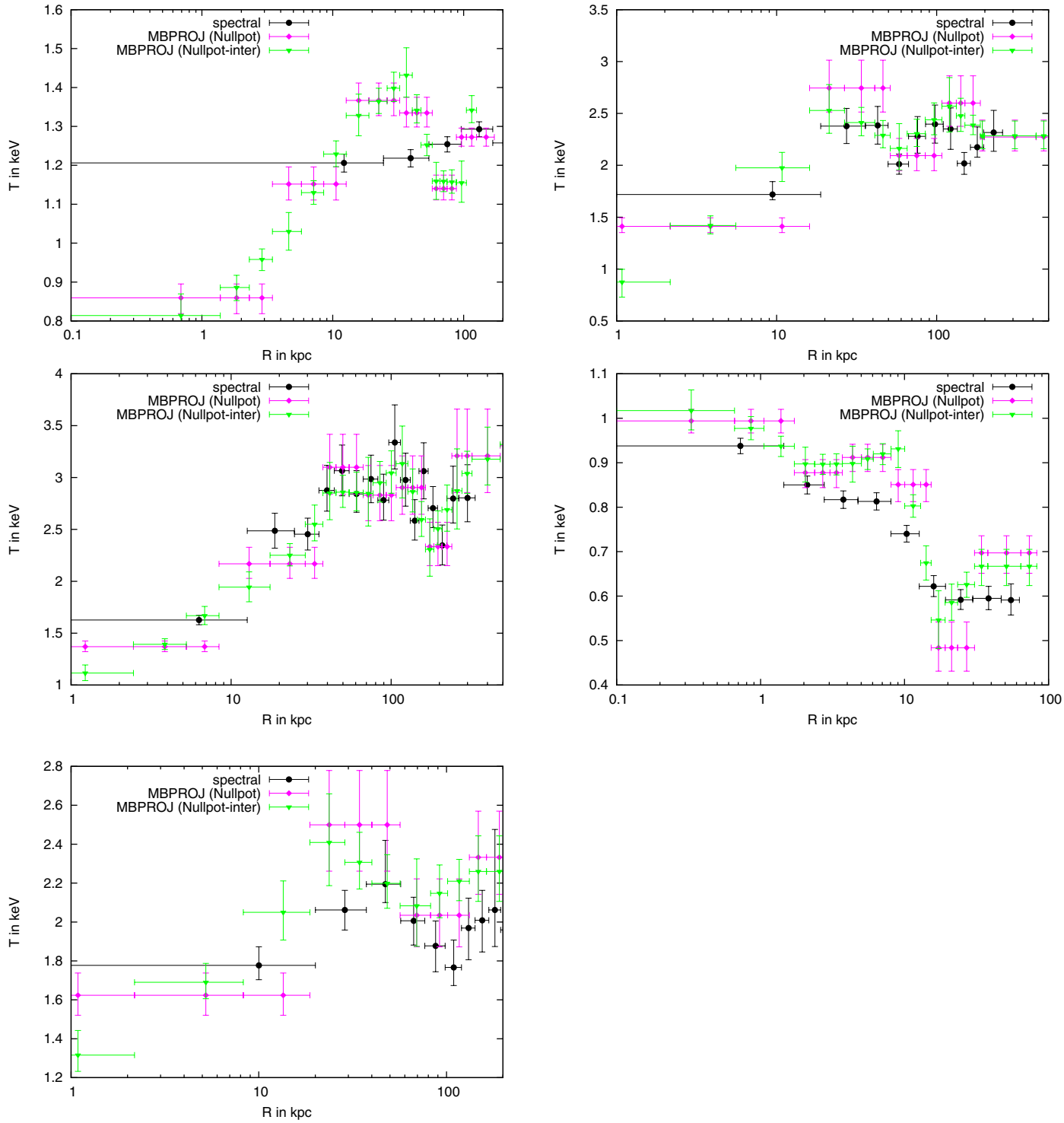

Fig. 3. Temperature profiles of the fossil systems, from spectral analysis and MBPROJ. *Clockwise from top left*: NGC 1132, RXJ 0454.8-1806, NGC 6482, ESO306, UGC 00842. The spectral temperature profiles were also determined for an abundance of 0.3 $Z_{\odot}$.

different slopes and normalisations, and excising the core regions result in a lowered intrinsic scatter (e.g. Pratt et al. 2009; Mittal et al. 2011; Maughan et al. 2012). Along with cool-cores and possibly AGN feedback, selection effects can also play a significant role in determining "true" scaling relations as has been shown by several authors before (e.g. Ikebe et al. 2002; Stanek et al. 2006; Pacaud et al. 2007; Mantz et al. 2010; Mittal et al. 2011; Lovisari et al. 2015; Bharadwaj et al. 2015; also see Giodini et al. 2013 Sect. 7, for a review). Thus, simply using a sample of clusters/groups to construct scaling relations without accounting for potential selection effects would not result in an accurate description of the underlying properties of the objects. In this work, there are seven fossil systems from the 400d catalogue (out of 12). The 400d catalogue has fairly well-defined selection criteria, making it relatively easy to account for selection effects and study whether the $L_X - T$ scaling relation

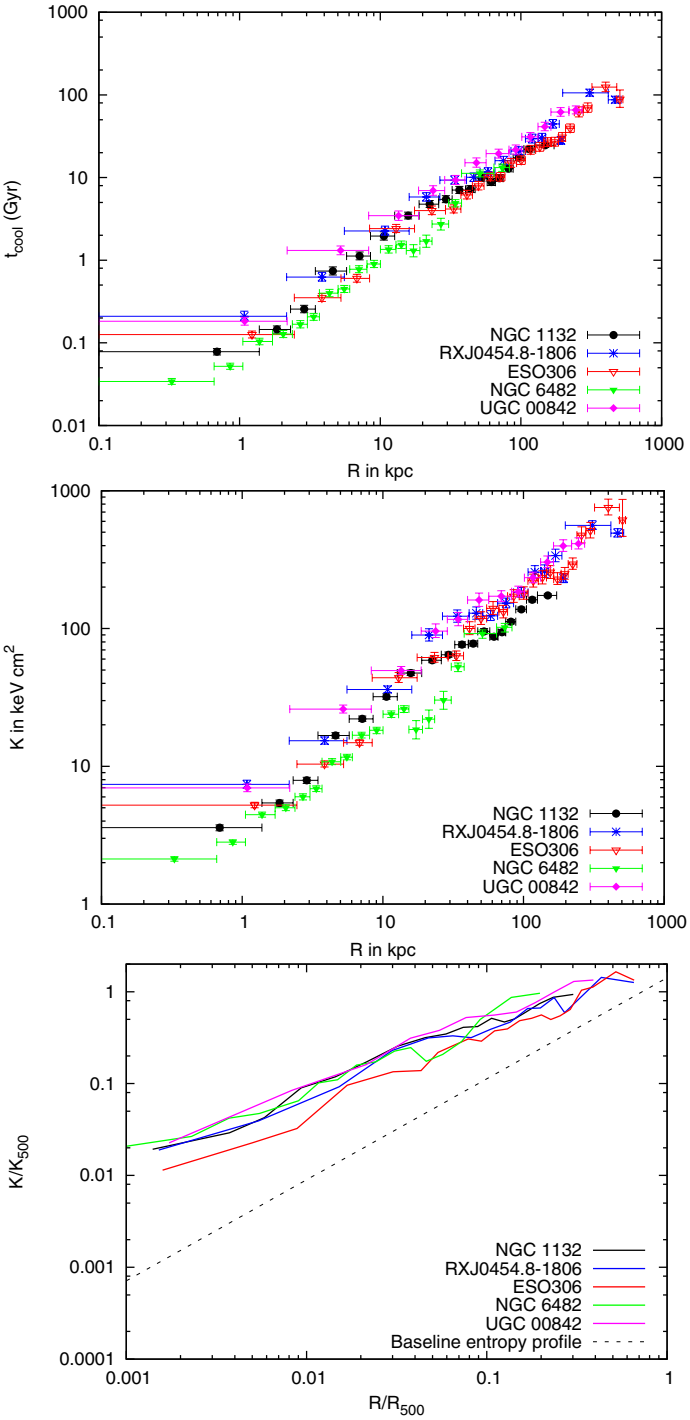

Fig. 4. *Top*: cooling time profiles of $z < 0.05$ fossils. *Middle*: entropy profiles of $z < 0.05$ fossils. Both quantities are obtained from the non-interpolated temperatures estimated from the MBPROJ code. *Bottom*: scaled entropy profiles. Dashed line represents the baseline entropy profile from Pratt et al. (2010).

for fossils show features that are different from non-fossils. To compare the results here, we used the groups in the Bharadwaj et al. (2015) study. To maintain consistency with that study, we used the best-fit virial temperatures and abundances of the fossils to convert the catalogue ROSAT (0.5–2.0 keV band) luminosities into bolometric luminosities (0.01–40 keV band).

To determine the scaling relation, we used the BCES (Y|X) code by Akritas & Bershady (1996) and the fits were performed in Log space using the fitting function, i.e.

$$\left(\frac{L_{\rm X}(0.01-40\ {\rm keV})}{0.5\times10^{44}\ {\rm erg\ s^{-1}}}\right) = c\times\left(\frac{T}{3\ {\rm keV}}\right)^{m}. \quad (19)$$

This yields a slope of 2.09 ± 0.24 and normalisation (log) of 0.29 ± 0.04. The observed scaling relation for groups in the Bharadwaj et al. (2015) study has a slope of 2.17 ± 0.26 and normalisation of -0.01 ± 0.09. To ensure that our choice of region for the temperature determination was not biasing our results, we performed a test by estimating the temperatures in a fixed region of 3 arcmin for all the 400d fossils (effectively corresponding to a median of $\sim 0.5 r_{500}$) and redid the scaling relation. No significant changes were found. The observed scaling relation provides first indications that fossils seem to be more X-ray luminous for a given T (Fig. 5, left), relative to non-fossils, although this could simply be as a result of selection effects.

To investigate this further, we performed an additional test where we froze the slopes for both the fossils and groups to 3.0 and only fit the normalisation for both samples. The value of 3.0 for the slope was chosen as generally most groups and clusters can be described well by this particular slope, after factoring in selection effects. The fossils now have a normalisation of 0.38 ± 0.11 and the groups sample have a normalisation of 0.22 ± 0.13. We now proceeded to remove the influence of selection effects on the normalisation of the scaling relation for both samples by generating mock samples of objects as in Bharadwaj et al. (2015) by varying the input normalisations. For each mock sample, the slope was always fixed to 3 and the intrinsic scatter was fixed to the observed values. Flux and luminosity cuts were applied to both the 400d sample and the groups sample to match the true sample of objects. For the 400d fossil sample, the selection criteria were taken from Voevodkin et al. (2010), and can be described as follows: a lower flux cut of 1.4×10^{-13} erg/s/cm^2, an upper redshift cut of 0.2, and a lower luminosity cut of 10^{43} erg/s. Here, fluxes and luminosities are in the ROSAT (0.5–2.0 keV) band. After performing the bias corrections, the fossils scaling relation has a normalisation of 0.30 ± 0.10 vs. 0.0078 ± 0.13 for the groups, indicating that the large normalisations seem to persist even after accounting for selection effects. Despite a nearly 2.3σ higher normalisation for fossils with respect to non-fossils, we still only treat this finding as an indication because on top of the statistical uncertainties in both quantities (which is large currently for the 400d fossils), there could also be an additional systematic uncertainty introduced due to differences in the luminosity determination in the different parent catalogues. Secondly, the archival nature of this subsample of 400d objects is biased towards systems lacking a SCC (Table 2) and, assuming that the remaining systems are SCC, then adding these objects could potentially increase the normalisation for the scaling relation, and the difference between the fossils and the groups sample would be higher than what we demonstrate here. We plan to explore this in greater detail in a future study of fossils scaling relations.

3.7. Discussion

Though our results mostly concern the cores of fossil systems, these properties offer us interesting insights into their formation and evolution. Fossil systems not having experienced any recent major merger activity should have a pronounced cool-core with very short CCTs and "typical" temperature profiles

Table 5. Best-fit results for entropy profiles of $z < 0.05$ fossils, without and with core component.

Name	m	Normalisation (K_{100}, keV cm^2)	K_0 keV cm^2
NGC 6482	0.74 ± 0.04	103.3 ± 13.12	–
NGC 1132	0.75 ± 0.02	138.9 ± 6.08	–
RX J0454.8-1806	0.72 ± 0.02	184.2 ± 9.83	–
ESO 306-G 017	0.83 ± 0.02	170.1 ± 9.00	–
UGC 842	0.75 ± 0.02	224.49 ± 8.45	–
All 5 groups	0.80 ± 0.01	146.1 ± 5.41	–
NGC 6482	0.91 ± 0.05	139.7 ± 16.3	1.24 ± 0.29
NGC 1132	0.70 ± 0.04	138.9 ± 5.96	−1.38 ± 1.30
RX J0454.8-1806	0.72 ± 0.05	184.5 ± 11.1	−0.14 ± 2.38
ESO 306-G 017	0.90 ± 0.04	168.9 ± 8.25	1.83 ± 0.84
UGC 842	0.70 ± 0.03	225.1 ± 7.72	−2.43 ± 1.53
All 5 groups	0.84 ± 0.02	147.5 ± 5.38	0.74 ± 0.36

Notes. Columns are (1) name of group; (2) slope; (3) normalisation; (4) core entropy.

Table 6. Comparison of the "bias-corrected" scaling relations for the 400d fossils and the Bharadwaj et al. (2015) sample by freezing the slope to 3.

Sample	Slope	Normalisation (observed)	Normalisation (bias-corrected)
400d fossils	3	0.38 ± 0.10	0.30 ± 0.10
Groups sample	3	0.22 ± 0.13	0.0078 ± 0.13

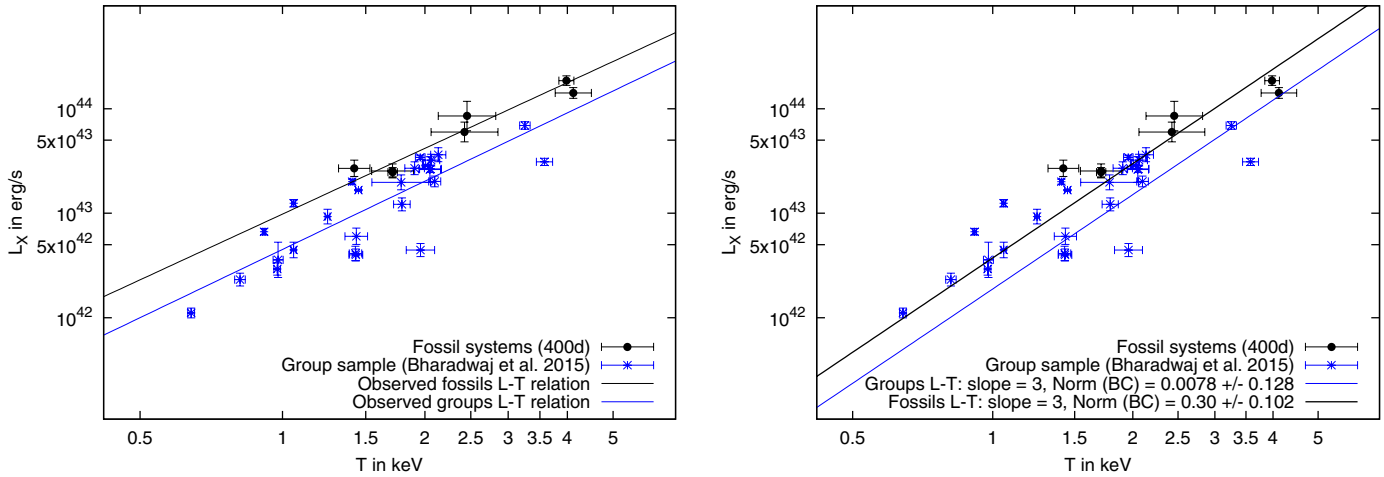

Fig. 5. *Left*: observed $L_X - T$ relation for 400d fossils and groups sample. *Right*: comparison of 400d fossil $L_X - T$ relation and groups relation with frozen slope and bias-corrected normalisations.

with a clear central temperature drop. The distribution of the CCTs and the shapes of the observed temperature profiles does not, however, seem to support this idea. Given that the BCG-EP separation is not large and that most fossils still have an EP-EWC separation less than 50 kpc, it seems unlikely that invoking mergers can easily explain the thermodynamic properties of the fossils.

A lot of these properties can be explained as a result of a non-gravitational process, in particular, the AGN activity at the fossil centres which we speculate was much more powerful at an earlier epoch than it is now. Simulation results by e.g. Dariush et al. (2007) and Díaz-Giménez et al. (2011) point out that fossils assemble most of their masses at high redshifts. Interestingly, Díaz-Giménez et al. (2008) point out that while the virial mass of the groups were assembled at high redshifts, much of the BCG mass is assembled at much later epochs. Recent results by Méndez-Abreu et al. (2012) conclude that the BCGs of fossils underwent major dissipational mergers at earlier epochs, albeit most of the stellar content was assembled via dissipationless major mergers at later times. Thus, we speculate that during the relatively "gas-rich" phase of mass assembly, the supermassive black hole (SMBH) was strongly fuelled, which led to strong AGN feedback such that an almost isothermal central region, or a centrally rising temperature profile was formed. When this phase ended, dissipationless major mergers continued to build the BCG, but there was not enough gas to fuel the SMBH strongly, pushing it into a state of relative quiescence. Eventually, for some objects, a small cool-core region was formed probably from the mixture of stellar mass ejecta and the surrounding ICM, not quite unlike thermal coronae seen in groups/clusters. This cool gas started feeding the SMBH, and is now probably involved in a self-regulated feedback cycle, which

leads to a much lower AGN activity (e.g. Gaspari 2015). Four out of the five $z < 0.05$ fossils show extremely weak radio sources (Bharadwaj et al. 2014; Miraghaei et al. 2014; Condon et al. 1998) indicating that the AGN activity is definitely not strong currently, giving credence to this theory. Interestingly, simulation results by Burns et al. (2008) indicate that non-cool core clusters (cool cores here are defined by a central temperature drop in the temperature profile) at low redshifts ($z < 0.3$) have fewer halos in their neighbourhood as compared to CC clusters, while the situation was exactly reversed at $z > 1$. Though Burns et al. (2008) only discuss clusters with virial masses greater than 10^{14} $M_{\odot}$, the under dense regions of fossil systems relative to other systems would seem to qualitatively agree with the idea that the progenitors of fossils originated in a region with a higher density of halos that strongly contributed to mergers, and the final mass assembly currently resides in a relatively under-dense region. This is also qualitatively in agreement with the observational results of Harrison et al. (2012), who base their conclusions via a study of the fossil ellipticals and the simulation results of Díaz-Giménez et al. (2011).

The above speculation however, still does not explain the "classical" temperature profile seen for cl1159p5531 and the high-temperature fossils. One possibility is that the thermodynamic properties of the fossil systems are strongly dependent on the environment in which it was formed. These anomalous objects could have grown in a region relatively under-dense in halos, which led to the formation of a proper cool-core via hierarchical, small-scale mergers (Burns et al. 2008) and relatively gentle AGN feedback throughout. Secondly, we do not rule out the possibility of the high-temperature objects falsely identified as fossils, as the Eigenthaler & Zeilinger (2009) sample is largely based on the SDSS catalogue and it has been known for some systems to be wrongly classified as fossils in similar studies, only to be corrected later when better data was available (e.g. Zarattini et al. 2014 vs. Santos et al. 2007). Cl1159p5531 has a galaxy just outside the search radius, which if included would not satisfy the magnitude criterion of Voevodkin et al. (2010) and be classified as a fossil in that study. Naively though, it seems unlikely that subtle changes in the magnitude gap would have a drastic impact on the ICM properties of these objects.

4. Summary

We have studied the core properties of 17 fossil systems from literature with data from the *Chandra* archives. The conclusions of our work can be summarised as follows:

- Most fossil systems (82%) are identified as cool-core objects based on at least two diagnostics. Interestingly though, there are indications that most fossil systems are WCC objects and that the population of non-SCC fossils outstrip SCC fossils.
- Fossil systems show a large range of temperature profiles with some cool-core objects lacking the expected clear central temperature drop.
- We analysed the X-ray emission coincident with the BCG for fossils with $z < 0.1$ and conclude that these are not the typical X-ray coronae reported for some other objects. We speculate that the stellar X-ray component (if present) has mixed with the ICM.
- We performed a deprojection analysis using the SBPs for fossils with $z < 0.05$ and derived their thermodynamic properties. These objects lack group-sized cool-cores and show evidence for non-gravitational processes (AGN feedback in particular) based on the shallow power-law indices of their entropy profiles.
- There are some indications that the normalisation of the $L_X - T$ relation is higher for fossils than for non-fossils.
- We speculate that early, dissipational major mergers led to a strong fuelling of the central SMBH, leading to powerful AGN feedback, and this could explain the lack of group-sized cool-cores in low-temperature fossil groups. There are, however, anomalous cases, which lead us to conclude that this is probably an incomplete picture of the formation and evolution of fossil systems.

In short, we have offered a glimpse into the nature of fossil systems through their core properties. In order to concretise these ideas, we will have to construct large, objectively selected sample of fossils with high quality X-ray data; ideally with some mass/luminosity cut to distinguish between fossil groups and clusters. A key point here seems to be to also improve our understanding of the weak cool-core cluster/group regime, which to date has been probed poorly. These observational results will also need backing from detailed, high-resolution simulations, which factors into it feedback processes that would help us unravel substantial features in the growth of fossil systems and the impact on the properties of the ICM.

Acknowledgements. The authors would like to thank the referee for constructive feedback. V.B. would like to thank Lorenzo Lovisari for constructive comments. V.B. and G.S. acknowledge support from the DFG via grant RE 1462/6. T.H.R. acknowledges support from the DFG through the Heisenberg research grant RE 1462/5. The program for calculating the CCT was kindly provided by Paul Nulsen, which is based on spline interpolation on a table of values for the APEC model assuming an optical thin plasma by R.K. Smith. This work has made use of the NASA/IPAC extragalactic database (NED) which is operated by the Jet Propulsion Laboratory, California Institute of Technology, under contract with the National Aeronautics and Space Administration.

References

Akritas, M. G., & Bershady, M. A. 1996, ApJ, 470, 706
Anders, E., & Grevesse, N. 1989, Geochim. Cosmochim. Acta, 53, 197
Arnaud, M., Pointecouteau, E., & Pratt, G. W. 2005, A&A, 441, 893
Bharadwaj, V., Reiprich, T. H., Schellenberger, G., et al. 2014, A&A, 572, A46
Bharadwaj, V., Reiprich, T. H., Lovisari, L., & Eckmiller, H. J. 2015, A&A, 573, A75
Borm, K., Reiprich, T. H., Mohammed, I., & Lovisari, L. 2014, A&A, 567, A65
Burns, J. O., Hallman, E. J., Gantner, B., Motl, P. M., & Norman, M. L. 2008, ApJ, 675, 1125
Cavagnolo, K. W., Donahue, M., Voit, G. M., & Sun, M. 2009, ApJS, 182, 12
Cavaliere, A., & Fusco-Femiano, R. 1976, A&A, 49, 137
Condon, J. J., Cotton, W. D., Greisen, E. W., et al. 1998, AJ, 115, 1693
Dariush, A., Khosroshahi, H. G., Ponman, T. J., et al. 2007, MNRAS, 382, 433
Dariush, A. A., Raychaudhury, S., Ponman, T. J., et al. 2010, MNRAS, 405, 1873
Díaz-Giménez, E., Muriel, H., & Mendes de Oliveira, C. 2008, A&A, 490, 965
Díaz-Giménez, E., Zandivarez, A., Proctor, R., Mendes de Oliveira, C., & Abramo, L. R. 2011, A&A, 527, A129
D'Onghia, E., Sommer-Larsen, J., Romeo, A. D., et al. 2005, ApJ, 630, L109
Eckert, D., Molendi, S., & Paltani, S. 2011, A&A, 526, A79
Eckmiller, H. J., Hudson, D. S., & Reiprich, T. H. 2011, A&A, 535, A105
Eigenthaler, P., & Zeilinger, W. W. 2009, Astron. Nachr., 330, 978
Evrard, A. E., Metzler, C. A., & Navarro, J. F. 1996, ApJ, 469, 494
Fabian, A. C., Hu, E. M., Cowie, L. L., & Grindlay, J. 1981, ApJ, 248, 47
Gaspari, M. 2015, MNRAS, 451, L60
Giodini, S., Lovisari, L., Pointecouteau, E., et al. 2013, SSR, 177, 247
Harrison, C. D., Miller, C. J., Richards, J. W., et al. 2012, ApJ, 752, 12
Hudson, D. S., Reiprich, T. H., Clarke, T. E., & Sarazin, C. L. 2006, A&A, 453, 433
Hudson, D. S., Mittal, R., Reiprich, T. H., et al. 2010, A&A, 513, A37
Ikebe, Y., Reiprich, T. H., Böhringer, H., Tanaka, Y., & Kitayama, T. 2002, A&A, 383, 773
Jones, L. R., Ponman, T. J., Horton, A., et al. 2003, MNRAS, 343, 627

Kaastra, J. S., den Boggende, A. J., Brinkman, A. C., et al. 2001, in X-ray Astronomy 2000, eds. R. Giacconi, S. Serio, & L. Stella, ASP Conf. Ser., 234, 351
Kalberla, P. M. W., Burton, W. B., Hartmann, D., et al. 2005, A&A, 440, 775
Khosroshahi, H. G., Jones, L. R., & Ponman, T. J. 2004, MNRAS, 349, 1240
Khosroshahi, H. G., Ponman, T. J., & Jones, L. R. 2007, MNRAS, 377, 595
La Barbera, F., de Carvalho, R. R., de la Rosa, I. G., et al. 2009, AJ, 137, 3942
Lopes de Oliveira, R., Carrasco, E. R., Mendes de Oliveira, C., et al. 2010, AJ, 139, 216
Lovisari, L., Reiprich, T. H., & Schellenberger, G. 2015, A&A, 573, A118
Mantz, A., Allen, S. W., Ebeling, H., Rapetti, D., & Drlica-Wagner, A. 2010, MNRAS, 406, 1773
Maughan, B. J., Giles, P. A., Randall, S. W., Jones, C., & Forman, W. R. 2012, MNRAS, 421, 1583
Méndez-Abreu, J., Aguerri, J. A. L., Barrena, R., et al. 2012, A&A, 537, A25
Miller, E. D., Rykoff, E. S., Dupke, R. A., et al. 2012, ApJ, 747, 94
Miraghaei, H., Khosroshahi, H. G., Klöckner, H.-R., et al. 2014, MNRAS, 444, 651
Mittal, R., Hicks, A., Reiprich, T. H., & Jaritz, V. 2011, A&A, 532, A133
Mulchaey, J. S., & Zabludoff, A. I. 1999, ApJ, 514, 133
Pacaud, F., Pierre, M., Adami, C., et al. 2007, MNRAS, 382, 1289
Panagoulia, E. K., Fabian, A. C., & Sanders, J. S. 2014, MNRAS, 438, 2341
Pascut, A., & Ponman, T. J. 2015, MNRAS, 447, 3723
Peterson, J. R., Paerels, F. B. S., Kaastra, J. S., et al. 2001, A&A, 365, L104
Peterson, J. R., Kahn, S. M., Paerels, F. B. S., et al. 2003, ApJ, 590, 207
Pierini, D., Giodini, S., Finoguenov, A., et al. 2011, MNRAS, 417, 2927
Ponman, T. J., Allan, D. J., Jones, L. R., et al. 1994, Nature, 369, 462
Pratt, G. W., Croston, J. H., Arnaud, M., & Böhringer, H. 2009, A&A, 498, 361
Pratt, G. W., Arnaud, M., Piffaretti, R., et al. 2010, AAP, 511, A85
Proctor, R. N., de Oliveira, C. M., Dupke, R., et al. 2011, MNRAS, 418, 2054
Sanders, J. S., Fabian, A. C., Allen, S. W., et al. 2008, MNRAS, 385, 1186
Sanders, J. S., Fabian, A. C., Hlavacek-Larrondo, J., et al. 2014a, MNRAS, 444, 1497
Sanders, J. S., Fabian, A. C., Sun, M., et al. 2014b, MNRAS, 439, 1182
Santos, J. S., Rosati, P., Tozzi, P., et al. 2008, A&A, 483, 35
Santos, J. S., Tozzi, P., Rosati, P., & Böhringer, H. 2010, A&A, 521, A64
Santos, W. A., Mendes de Oliveira, C., & Sodré, J. L. 2007, AJ, 134, 1551
Schellenberger, G., Reiprich, T. H., Lovisari, L., Nevalainen, J., & David, L. 2015, A&A, 575, A30
Semler, D. R., Šuhada, R., Aird, K. A., et al. 2012, ApJ, 761, 183
Stanek, R., Evrard, A. E., Böhringer, H., Schuecker, P., & Nord, B. 2006, ApJ, 648, 956
Stott, J. P., Hickox, R. C., Edge, A. C., et al. 2012, MNRAS, 422, 2213
Sun, M., Forman, W., Vikhlinin, A., et al. 2004, ApJ, 612, 805
Sun, M., Jones, C., Forman, W., et al. 2007, ApJ, 657, 197
Sun, M., Voit, G. M., Donahue, M., et al. 2009, ApJ, 693, 1142
Tamura, T., Kaastra, J. S., Peterson, J. R., et al. 2001, A&A, 365, L87
Tozzi, P., & Norman, C. 2001, ApJ, 546, 63
Vikhlinin, A., McNamara, B. R., Hornstrup, A., et al. 1999, ApJ, 520, L1
Vikhlinin, A., Kravtsov, A., Forman, W., et al. 2006, ApJ, 640, 691
Vikhlinin, A., Burenin, R., Forman, W. R., et al. 2007, in Heating versus Cooling in Galaxies and Clusters of Galaxies, eds. H. Böhringer, G. W. Pratt, A. Finoguenov, & P. Schuecker (Berlin: Springer-Verlag), 48
Voevodkin, A., Miller, C. J., Borozdin, K., et al. 2008, ApJ, 684, 204
Voevodkin, A., Borozdin, K., Heitmann, K., et al. 2010, ApJ, 708, 1376
von Benda-Beckmann, A. M., D'Onghia, E., Gottlöber, S., et al. 2008, MNRAS, 386, 2345
Yoshioka, T., Furuzawa, A., Takahashi, S., et al. 2004, Adv. Space Res., 34, 2525
Zarattini, S., Barrena, R., Girardi, M., et al. 2014, A&A, 565, A116

Appendix A: Temperature profiles

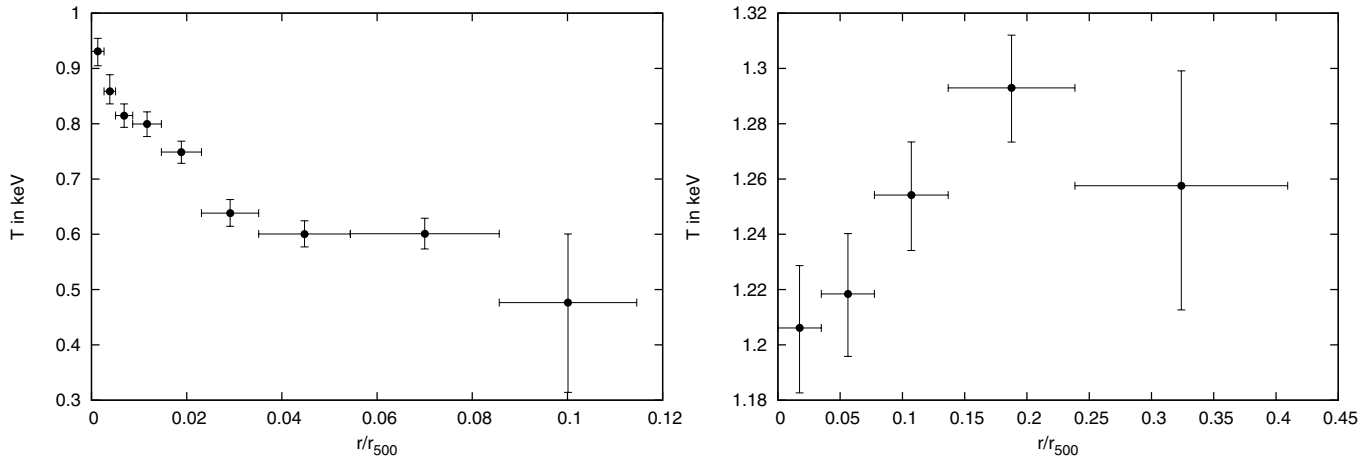

Fig. A.1. Temperature profiles of NGC 6482 and NGC 1132.

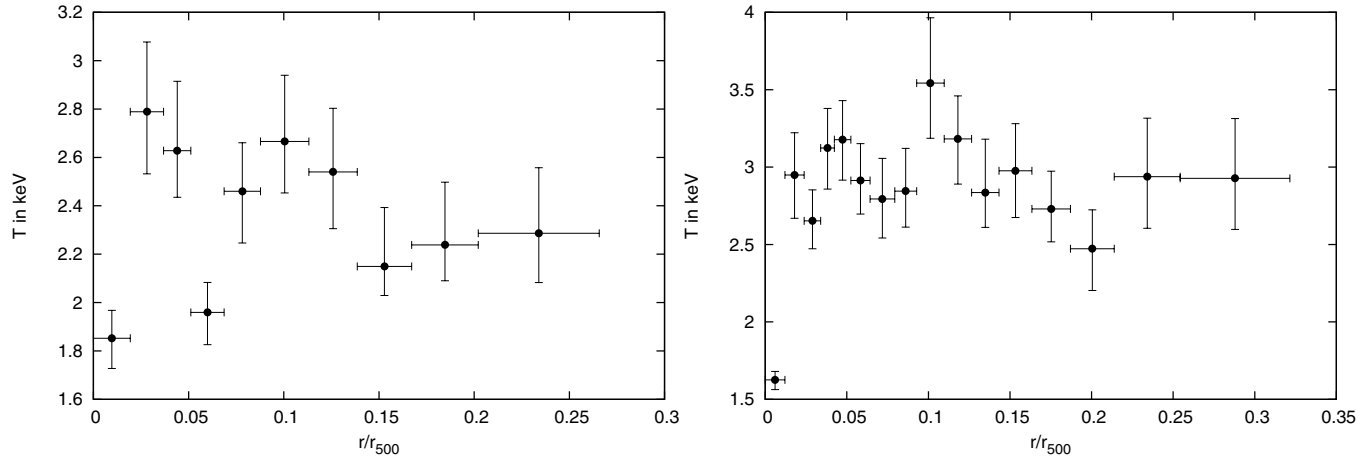

Fig. A.2. Temperature profiles of RX J0454.8-1806 and ESO306.

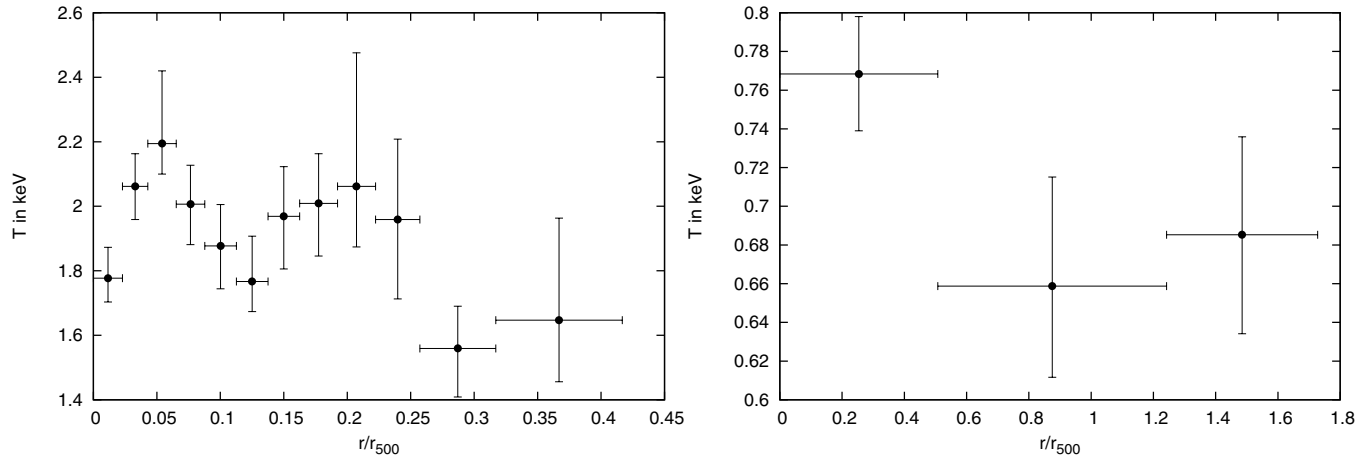

Fig. A.3. Temperature profiles of UGC 842 and RX J1331+1108. For RX J1331+1108, the blank-sky files might be under-estimating the background beyond r_{500}. This should however not be a problem in the central regions.

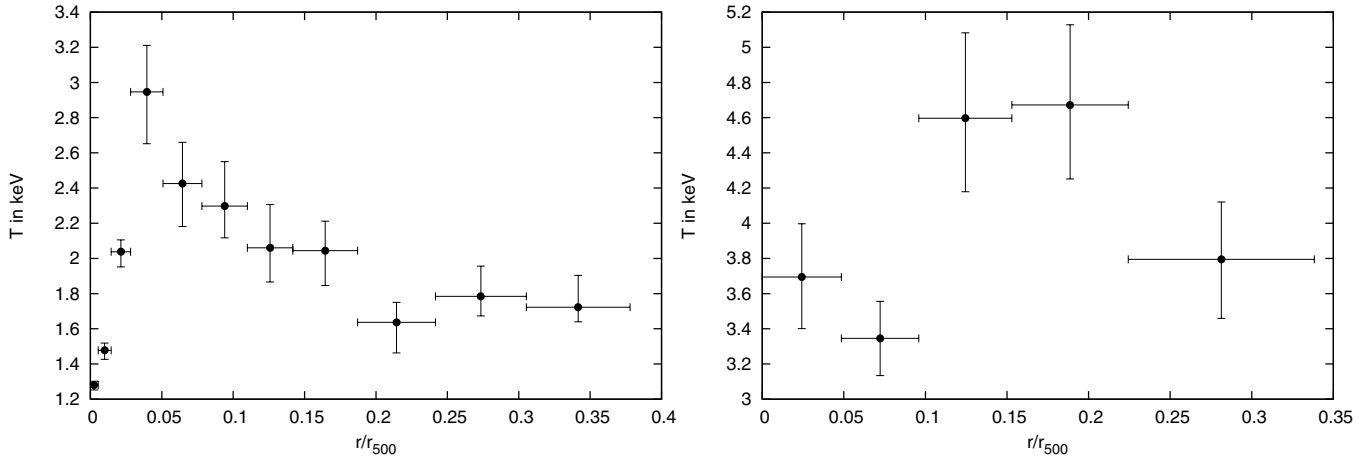

Fig. A.4. Temperature profiles of cl1159p5531 and cl1416p2315.

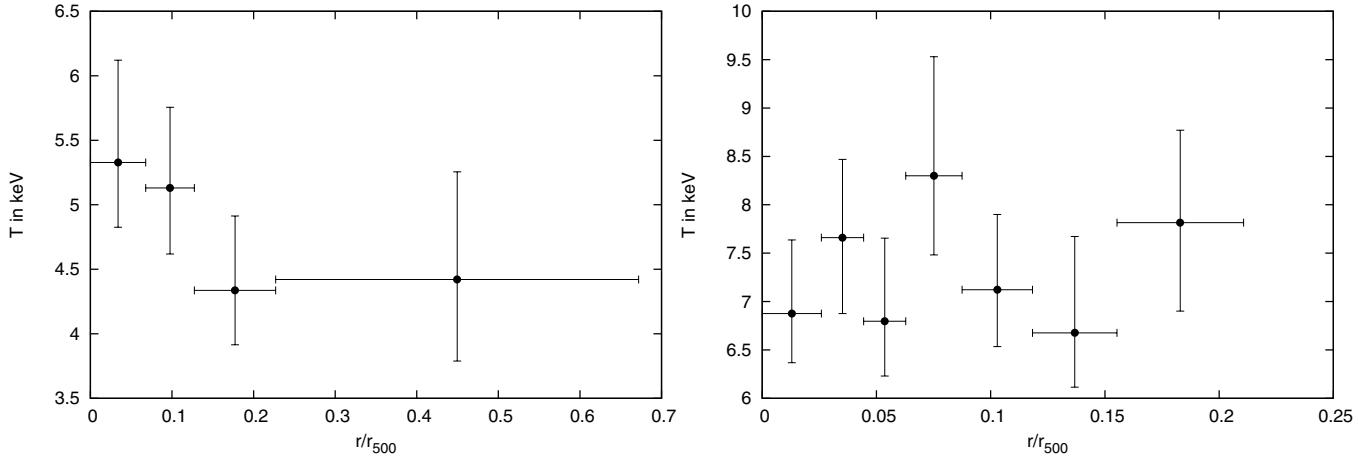

Fig. A.5. Temperature profiles of RX J0825.9+0415 and RX J0801+3603.

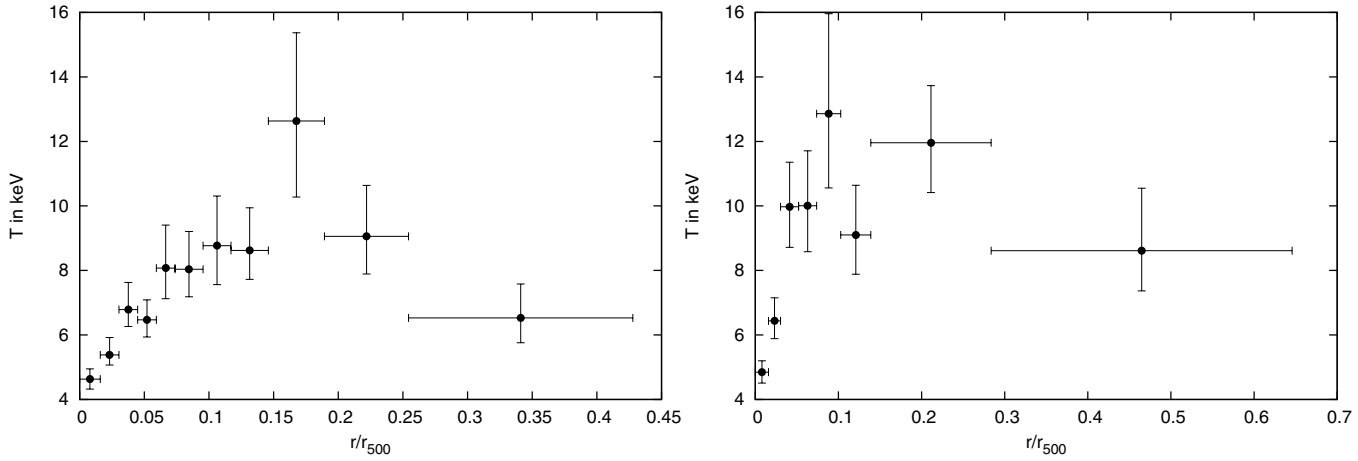

Fig. A.6. Temperature profiles of RX J1115.9+0130 and RX J0159.8-0850.